Inclusive deuteron electrodisintegration with polarized electrons and a polarized target

W. Leidemann
Istituto Nazionale di Fisica Nucleare, gruppo collegato di Trento, Dipartimento di Fisica, Università di Trento, I-38050 Povo, Italy

E.L. Tomusiak
Department of Physics and Saskatchewan Accelerator Laboratory, University of Saskatchewan, Saskatoon, Canada

H. Arenhövel
Institut für Kernphysik, Johannes Gutenberg-Universität Mainz, D-6500 Mainz, Federal Republic of Germany
(Received 1 October 1990)

Inclusive electrodisintegration of the deuteron with polarized beam and target is investigated in detail. The additional polarization form factors are derived and their decomposition into multipoles is given. The sensitivity of these form factors to the potential model, to subnuclear degrees of freedom, and to electromagnetic form factors is studied in different kinematical regions.

I. INTRODUCTION

The development of new experimental techniques and facilities will lead in the near future to more scattering experiments utilizing polarized electrons and/or polarized targets. Such experiments offer the possibility of new insights into the structure of nucleons and nuclei. In fact, the use of polarization observables in order to determine the neutron electric form factor G_{En} in electron scattering from light nuclei has already been extensively discussed.[1-5] However, apart from the question of determining G_{En} or from formal discussions of the nuclear response functions,[6,7] a detailed study of the dynamical properties of these polarization responses is still missing. In other words, there exists no study on how the various polarization observables are affected by the potential model, by meson and isobar degrees of freedom and if such observables would allow one to investigate the dynamical features of the nuclear system in much greater detail than is possible without the use of polarization.

With this work we will begin such a study for deuteron electrodisintegration utilizing polarized electrons and/or polarized targets. In a previous paper we have already presented the general formalism for the exclusive reaction.[3] However, there we were concerned only with the influence of G_{En} on various polarization observables and considered the deuteron merely as a neutron target. Here, however, we want to study the more general aspects and physical properties of the two-body system, e.g., NN potential model sensitivities and the importance of subnuclear degrees of freedom. We initiate this study by considering inclusive deuteron breakup which depends on only 10 form factors instead of the much more complex exclusive process $^2\vec{\mathrm{H}}(\vec{e},e'N)N$ with its 41 individual structure functions. The latter will be studied in the future.

In Sec. II we derive the formulas required for describing the $^2\vec{\mathrm{H}}(\vec{e},e')np$ process starting from the general formalism of Ref. 3. The above-mentioned 10 form factors will become apparent in the derivation. Explicit expressions in terms of the electromagnetic multipoles will be given, and we show how each of these form factors can be experimentally separated by choosing appropriate experimental conditions. Finally, we study in Sec. III the various form factors in three kinematical regions which are selected to represent different areas of sensitivities to the final-state interaction and to interaction currents mediated by meson exchange and Δ-degrees of freedom.

II. FORMALISM

The differential cross section for the coincidence reaction which includes both beam and target polarizations is given in Ref. 3 as

$$\frac{d^3\sigma}{dk_2^{lab}d\Omega_e^{lab}d\Omega_{np}^{c.m.}}$$

$$= c\Big\{ \rho_L f_L + \rho_T f_T + \rho_{LT} f_{LT}\cos\phi + \rho_{TT} f_{TT}\cos 2\phi + h\rho'_{LT} f'_{LT}\sin\phi$$
$$+ P_1^d\Big[(\rho_L f_L^{11} + \rho_T f_T^{11})d^1_{10}(\theta_d)\sin(\phi-\phi_d) + \sum_{M=-1}^{1}(\rho_{LT} f_{LT}^{1M}\sin\xi_M + \rho_{TT} f_{TT}^{1M}\sin\psi_M)d^1_{M0}(\theta_d)\Big]$$
$$+ P_2^d\Big[\sum_{M=0}^{2}(\rho_L f_L^{2M} + \rho_T f_T^{2M})d^2_{M0}(\theta_d)\cos[M(\phi-\phi_d)] + \sum_{M=-2}^{2}(\rho_{LT} f_{LT}^{2M}\cos\xi_M + \rho_{TT} f_{TT}^{2M}\cos\psi_M)d^2_{M0}(\theta_d)\Big]$$
$$+ hP_1^d\Big[\rho'_T\sum_{M=0}^{1} f_T'^{1M}\cos[M(\phi-\phi_d)]d^1_{M0}(\theta_d) + \rho'_{LT}\sum_{M=-1}^{1} f_{LT}'^{1M}\cos\xi_M d^1_{M0}(\theta_d)\Big]$$
$$+ hP_2^d\Big[\rho'_T\sum_{M=1}^{2} f_T'^{2M}\sin[M(\phi-\phi_d)]d^2_{M0}(\theta_d) + \rho'_{LT}\sum_{M=-2}^{2} f_{LT}'^{2M}\sin\xi_M d^2_{M0}(\theta_d)\Big]\Big\}, \quad (1)$$

with

$$c = \frac{\alpha}{6\pi^2}\frac{k_2^{\rm lab}}{k_1^{\rm lab}q_\nu^4}, \quad (2)$$

$$\xi_M = M(\phi-\phi_d)+\phi, \quad (3)$$

$$\psi_M = M(\phi-\phi_d)+2\phi. \quad (4)$$

The scattering geometry is illustrated in Fig. 1. Note that only longitudinally polarized electrons are considered. The quantities $\rho^{(\prime)}_{\lambda\mu}$ [primed and unprimed quantities, $\rho_{\lambda\mu}$ and $\rho'_{\lambda\mu}$, are here referred to collectively as $\rho^{(\prime)}_{\lambda\mu}$; a similar convention is used for $f^{(\prime)IM}_{\lambda\mu}$ and $F^{(\prime)IM}_{\lambda\mu}$] describe the virtual photon density matrix [$(\lambda\mu) = (00)$, (11), (01), and (−11) correspond to L, T, LT, and TT, respectively], h is the degree of longitudinal electron polarization, $k_1^{\rm lab}$ and $k_2^{\rm lab}$ denote the laboratory frame momenta of the initial and the scattered electrons, respectively, while q_ν^2 is the four-momentum transfer squared ($q = k_1 - k_2$). The structure functions $f^{(\prime)IM}_{\lambda\mu}$ ($f^{(\prime)00}_{\lambda\mu} \equiv f^{(\prime)}_{\lambda\mu}$) are all calculated in the final n-p c.m. system to which also $\Omega_{np}^{\rm c.m.} = (\theta,\phi)$, the spherical angles of the relative n-p momentum, refers. Effects of the boost from the laboratory to the c.m. system are included in the virtual photon density matrix which thus has to be evaluated in the c.m. system leading to

$$\rho_L = \beta^2 q_\nu^2\frac{\xi^2}{2\eta}, \quad \rho_{LT} = \beta q_\nu^2\frac{\xi}{\eta}\sqrt{\frac{\xi+\eta}{8}}, \quad (5)$$

$$\rho_T = \frac{1}{2}q_\nu^2\left(1+\frac{\xi}{2\eta}\right), \quad \rho_{TT} = -q_\nu^2\frac{\xi}{4\eta}, \quad (6)$$

$$\rho'_{LT} = \frac{1}{2}\beta q_\nu^2\frac{\xi}{\sqrt{2\eta}}, \quad \rho'_{TT} = \frac{1}{2}q_\nu^2\sqrt{\frac{\xi+\eta}{\eta}}, \quad (7)$$

with

$$\beta = \frac{|\mathbf{q}_{\rm lab}|}{|\mathbf{q}_{\rm c.m.}|}, \quad \xi = \frac{q_\nu^2}{\mathbf{q}^2_{\rm lab}}, \quad \eta = \tan^2\left(\frac{\theta_e^{\rm lab}}{2}\right), \quad (8)$$

where β expresses the boost from the lab to the c.m. system. The deuteron target is characterized by vector and tensor polarization parameters P_1^d and P_2^d, respectively, and by the angles θ_d and ϕ_d. The latter describe the direction of the orientation axis $\hat{\mathbf{d}}$ of the polarized deuteron target with respect to the coordinate system associated with the momentum transfer $\hat{\mathbf{q}}$ (see Fig. 1). $\hat{\mathbf{d}}$ is the axis with respect to which the deuteron density matrix is diagonal. Note that the deuteron density matrix undergoes no change in transforming from the lab to the c.m. system, since the boost is along $\hat{\mathbf{q}}$.[8]

The functions $f^{(\prime)IM}_{\lambda\mu}$ are proportional to either the real

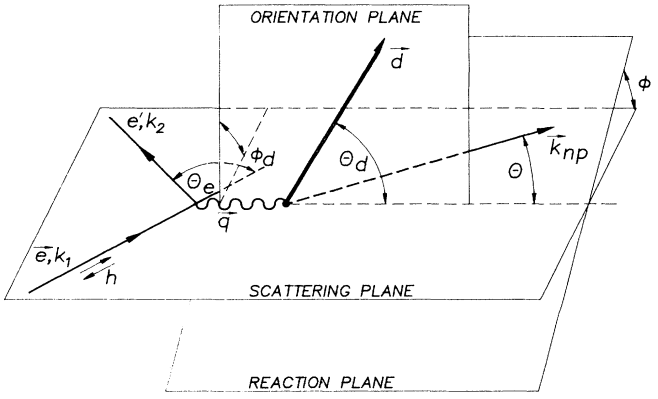

FIG. 1. Geometry of exclusive electron-deuteron scattering with polarized electrons and oriented deuteron target. Relative n-p momentum is denoted by $\mathbf{k}_{np}$ characterized by angles θ and ϕ and deuteron orientation axis by $\vec{d}$ characterized by angles θ_d and ϕ_d.

or imaginary parts of the quantities

$$v_{\lambda\mu IM}(\theta) = \hat{I}\sqrt{3}\sum_{m_d m'_d}(-)^{1-m_d}\begin{pmatrix}1 & 1 & I\\ m_d & -m'_d & -M\end{pmatrix} \times \sum_{sm_s} t^*_{sm_s\lambda m'_d}(\theta)t_{sm_s\mu m_d}(\theta)\ , \tag{9}$$

where $t_{sm_s\mu m_d}$ is the reduced transition matrix (i.e., the ϕ dependence has been separated) for the process $d+e\rightarrow np+e'$. In detail one has[3]

$$f^{IM}_{\lambda\mu} = \frac{4(-)^{1+\delta_{I0}}}{(1+\delta_{\lambda,-\mu})(1+\delta_{M0}\delta_{\lambda\mu})}\mathrm{Re}(i^{-I}v_{\lambda\mu IM})\ , \tag{10}$$

$$f'^{IM}_{\lambda\mu} = \frac{4(-)^{\delta_{I0}}}{(1+\delta_{M0}\delta_{\lambda\mu})}\mathrm{Im}(i^{I}v_{\lambda\mu IM})\ . \tag{11}$$

Reference 3 should be consulted for a detailed description of all the terms in (1).

The inclusive cross section is obtained by integration over the solid angle $\Omega^{\mathrm{c.m.}}_{np}$ which eliminates all terms with an explicit dependence on the azimuthal angle ϕ in (1). We define the inclusive form factors $F^{(\prime)IM}_{\lambda\mu}$ for the remaining terms by

$$F^{(\prime)IM}_{\lambda\mu} = \frac{1}{6}\int d\Omega f^{(\prime)IM}_{\lambda\mu} = \frac{\pi}{3}\delta_{\lambda-\mu,M}\int d(\cos\theta) f^{(\prime)IM}_{\lambda\mu}\ . \tag{12}$$

The introduction of the $v_{\lambda\mu IM}$ of (9) leads to

$$F^{IM}_{\lambda\mu} = \frac{\pi}{3(1+\delta_{\lambda,-\mu})}[(1-\delta_{I,1})\mathrm{Re}(I^{IM}_{\lambda\mu}) - \delta_{I,1}\mathrm{Im}(I^{IM}_{\lambda\mu})]\ , \tag{13}$$

$$F'^{IM}_{\lambda\mu} = \frac{\pi}{3}[\delta_{I,1}\mathrm{Re}(I^{IM}_{\lambda\mu}) - (1-\delta_{I,1})\mathrm{Im}(I^{IM}_{\lambda\mu})]\ , \tag{14}$$

with

$$I^{IM}_{\lambda\mu} = \frac{4\delta_{\lambda-\mu,M}}{(1+\delta_{M0}\delta_{\lambda\mu})}\int d(\cos\theta)\, v_{\lambda\mu IM}(\theta)\ . \tag{15}$$

We will now use the explicit multipole expansion for the t matrix as given essentially by Fabian and Arenhövel[9]

$$t_{sm_s\mu m_d} = (-)^{\mu}\sqrt{1+\delta_{\mu 0}}\sum_{Ljm_j\lambda}\hat{j}(1m_dL\mu|jm_j)(l0sm_s|jm_s)\mathcal{O}^{L\mu}(\lambda jls)d^j_{m_jm_s}(\theta)\ , \tag{16}$$

where

$$\mathcal{O}^{L\mu}(\lambda jls) = \sqrt{4\pi}\, e^{i\delta^j_\lambda}U^j_{ls,\lambda}N^L_\mu(\lambda j)\ , \tag{17}$$

and

$$N^L_\mu(\lambda j) = \delta_{|\mu|1}(E^L(\lambda j) + \mu M^L(\lambda j)) + \delta_{\mu 0}C^L(\lambda j)\ . \tag{18}$$

The only difference to Ref. 9 is that in (16) the deuteron quantization axis is taken along the momentum transfer $\hat{\mathbf{q}}$. The integration over θ can be performed explicitly and one finds

$$I^{IM}_{\mu'\mu} = (-)^{1+\mu}\frac{32\pi\hat{I}\sqrt{3}}{(1+\delta_{M0}\delta_{\mu'\mu})}\sqrt{(1+\delta_{\mu 0})(1+\delta_{\mu' 0})}\sum_{LL'j\lambda}(-)^j\begin{pmatrix}L' & L & I\\ \mu' & -\mu & -M\end{pmatrix}\begin{Bmatrix}L' & L & I\\ 1 & 1 & j\end{Bmatrix}N^{L'}_{\mu'}(\lambda j)^*N^L_\mu(\lambda j)\ . \tag{19}$$

The resulting expressions for the multipole decomposition of the form factors are listed explicitly in the Appendix.

We would like to point out that the above result only contains interference terms between transitions which lead to the same partial wave λj of the final state. The radial integrals $N^L_\mu(\lambda j)$ are real below pion threshold. This is a reflection of time-reversal invariance. Notice, therefore, that in this case all quantities $I^{IM}_{\lambda\mu}$ are real. A consequence of this is that the two form factors F^{1-1}_{LT} and F'^{2-1}_{LT}, which survived the integration over ϕ, must vanish. However, they do not vanish above pion threshold since $N^L_\mu(\lambda j)$ can become complex because of Δ- and real pion degrees of freedom.

The inclusive cross section for a polarized beam and target is then given explicitly by

$$\begin{aligned}\frac{d^2\sigma}{dk^{\mathrm{lab}}_2 d\Omega^{\mathrm{lab}}_e} = 6c\{&\rho_L F_L + \rho_T F_T + P^d_1\rho_{LT}F^{1-1}_{LT}\sin\phi_d d^1_{-10}(\theta_d)\\ &+P^d_2[(\rho_L F^{20}_L + \rho_T F^{20}_T)d^2_{00}(\theta_d) + \rho_{LT}F^{2-1}_{LT}\cos\phi_d d^2_{-10}(\theta_d) + \rho_{TT}F^{2-2}_{TT}\cos 2\phi_d d^2_{-20}(\theta_d)]\\ &+hP^d_1[\rho'_T F'^{10}_T d^1_{00}(\theta_d) + \rho'_{LT}F'^{1-1}_{LT}\cos\phi_d d^1_{-10}(\theta_d)] + hP^d_2\rho'_{LT}F'^{2-1}_{LT}\sin\phi_d d^2_{-10}(\theta_d)\}\\ \equiv\ &\sigma(h, P^d_1, P^d_2).\end{aligned} \tag{20}$$

and it depends on the ten form factors: F_L, F_T, F^{1-1}_{LT}, F^{20}_L, F^{20}_T, F^{2-1}_{LT}, F^{2-2}_{TT}, F'^{10}_T, F'^{1-1}_{LT}, and F'^{2-1}_{LT}, of which F^{1-1}_{LT}

and $F_{LT}^{\prime 2-1}$ vanish below pion threshold.

Parenthetically, we would like to mention that at the photon point one has the following equations which relate the purely transverse form factors to (a) the total photoabsorption cross section $\sigma_{\rm tot}$ of deuteron photodisintegration for unpolarized photons and deuterons and to (b) the corresponding photon and target asymmetries of the total cross section[10]

$$\sigma_{\rm tot} = \frac{M_d}{2E\omega} F_T \ , \quad \tau_{20}^0 = \frac{F_T^{20}}{F_T} \ , \tag{21}$$

$$\tau_{10}^c = \frac{F_T^{\prime 10}}{F_T} \ , \quad \tau_{22}^l = \frac{F_{TT}^{2-2}}{F_T} \ , \tag{22}$$

where E and ω denote respectively the total n-p and the photon c.m. energies.

The form factors in (20) can be separated by introducing various asymmetries and by selecting specific polarization angles θ_d and ϕ_d. In analogy to the asymmetries we defined for the exclusive deuteron breakup[3] we write the cross section in the form

$$\sigma(h,\, P_1^d,\, P_2^d) = \sigma_0[1 + P_1^d \alpha_d^V + P_2^d \alpha_d^T + h(P_1^d \alpha_{ed}^V + P_2^d \alpha_{ed}^T)] \ , \tag{23}$$

where

$$\sigma_0 = 6c(\rho_L F_L + \rho_T F_T) \ . \tag{24}$$

The various asymmetries are functions of the deuteron orientation angles (θ_d, ϕ_d), and they can be obtained from specific combinations of experimental settings as follows

$$\begin{aligned} \alpha_d^V(\theta_d, \phi_d) &= \frac{1}{2P_1^d \sigma_0}[\sigma(0,\, P_1^d,\, P_2^d) - \sigma(0,\, -P_1^d,\, P_2^d)] \\ &= \frac{6c}{\sigma_0} \rho_{LT} F_{LT}^{1-1} \sin\phi_d d^1_{-10}(\theta_d) \ , \end{aligned} \tag{25}$$

$$\begin{aligned} \alpha_d^T(\theta_d, \phi_d) &= \frac{1}{2P_2^d \sigma_0}[\sigma(0,\, P_1^d,\, P_2^d) + \sigma(0,\, -P_1^d,\, P_2^d) - 2\sigma_0] \\ &= \frac{6c}{\sigma_0}[(\rho_L F_L^{20} + \rho_T F_T^{20}) d^2_{00}(\theta_d) + \rho_{LT} F_{LT}^{2-1} \cos\phi_d d^2_{-10}(\theta_d) + \rho_{TT} F_{TT}^{2-2} \cos 2\phi_d d^2_{-20}(\theta_d)] \ , \end{aligned} \tag{26}$$

$$\begin{aligned} \alpha_{ed}^V(\theta_d, \phi_d) &= \frac{1}{4hP_1^d \sigma_0}[\sigma(h, P_1^d, P_2^d) - \sigma(-h, P_1^d, P_2^d) - \sigma(h, -P_1^d, P_2^d) + \sigma(-h, -P_1^d, P_2^d)] \\ &= \frac{6c}{\sigma_0}[\rho'_T F_T^{\prime 10} d^1_{00}(\theta_d) + \rho'_{LT} F_{LT}^{\prime 1-1} \cos\phi_d d^1_{-10}(\theta_d)] \ , \end{aligned} \tag{27}$$

$$\begin{aligned} \alpha_{ed}^T(\theta_d, \phi_d) &= \frac{1}{4hP_2^d \sigma_0}[\sigma(h, P_1^d, P_2^d) - \sigma(-h, P_1^d, P_2^d) + \sigma(h, -P_1^d, P_2^d) - \sigma(-h, -P_1^d, P_2^d)] \\ &= \frac{6c}{\sigma_0} \rho'_{LT} F_{LT}^{\prime 2-1} \sin\phi_d d^2_{-10}(\theta_d) \ . \end{aligned} \tag{28}$$

As usual F_L and F_T are determined from a Rosenbluth separation of the unpolarized cross section. Furthermore, F_{LT}^{1-1} and $F_{LT}^{\prime 2-1}$ are easily obtained from α_d^V and α_{ed}^T, respectively. Since these two form factors vanish below pion threshold, it follows in this case that, on the one hand, without electron polarization the inclusive cross section does not depend on the deuteron vector polarization and, on the other hand, that for a tensor polarized deuteron target additional electron polarization does not carry new information.

Somewhat more complicated is the asymmetry α_d^T, since it depends on four form factors. One possibility for separating them is to use the explicit ϕ_d dependence. For example, choosing consecutively $\phi_d = 0, \frac{\pi}{2}$, and π one finds the following relations:

$$\begin{aligned} &\tfrac{1}{2}[\alpha_d^T(\theta_d, 0) + \alpha_d^T(\theta_d, \pi)] + \alpha_d^T\left(\theta_d, \frac{\pi}{2}\right) \\ &\qquad = \frac{12c}{\sigma_0}(\rho_L F_L^{20} + \rho_T F_T^{20}) d^2_{00}(\theta_d) \ , \end{aligned} \tag{29}$$

$$\alpha_d^T(\theta_d,0)-\alpha_d^T(\theta_d,\pi)=\frac{12c}{\sigma_0}\rho_{LT}F_{LT}^{2-1}d^2_{-10}(\theta_d)\ , \tag{30}$$

$$\tfrac{1}{2}[\alpha_d^T(\theta_d,0)+\alpha_d^T(\theta_d,\pi)]-\alpha_d^T\left(\theta_d,\frac{\pi}{2}\right)=\frac{12c}{\sigma_0}\rho_{TT}F_{TT}^{2-2}d^2_{-20}(\theta_d)\ . \tag{31}$$

While F_{LT}^{2-1} and F_{TT}^{2-2} can be directly obtained from (30) and (31), F_L^{20} and F_T^{20} can be separated from (29) by the Rosenbluth technique. Another possibility rests on the fact that $d^2_{00}(\theta_d^0)=0$ for $\theta_d^0=\cos^{-1}(1/\sqrt{3})\simeq 54.7°$ and one finds that F_{LT}^{2-1} and F_{TT}^{2-2} can be determined from $\alpha_d^T(\theta_d^0,\pi/4)$ and $\alpha_d^T(\theta_d^0,\pi/2)$, respectively, i.e.,

$$\alpha_d^T\left(\theta_d^0,\frac{\pi}{4}\right)=-\frac{\sqrt{6}c}{\sigma_0}\rho_{LT}F_{LT}^{2-1}\ , \tag{32}$$

$$\alpha_d^T\left(\theta_d^0,\frac{\pi}{2}\right)=-\frac{\sqrt{6}c}{\sigma_0}\rho_{TT}F_{TT}^{2-2}\ . \tag{33}$$

Furthermore, for $\theta_d=0$ one finds that to the asymmetry

$$\alpha_d^T(0,\phi_d)=\frac{6c}{\sigma_0}(\rho_L F_L^{20}+\rho_T F_T^{20}) \tag{34}$$

only F_L^{20} and F_T^{20} contribute, and thus again the Rosenbluth technique will separate them. Finally, the beam-vector-target asymmetry is used to obtain the remaining form factors $F_T^{\prime 10}$ and $F_{LT}^{\prime 1-1}$ from α_{ed}^V at $\theta_d=0$ and $\theta_d=\pi/2$.

III. RESULTS AND DISCUSSION

We study the various form factors $F_{\lambda\mu}^{(\prime)IM}$ within a nonrelativistic framework as described in detail in Ref. 9. The only difference to Ref. 9 is that we do not use the nonrelativistic approximation in the kinematical factors of the T matrix as given in Eq. (61) of Ref. 3 but take instead the relativistic expressions. In the calculation of the t-matrix elements we use a multipole decomposition and include the final-state interaction up to the multipole order $L=6$. For the higher multipoles we use the Born approximation. This was shown to be a reliable procedure in Ref. 9. For the deuteron and n-p scattering wave functions we use the same potential models as employed in our study of the role of G_{En} in the exclusive deuteron breakup, namely the Paris,[11] Bonn[12] (r-space version), and Argonne V_{14} and V_{28} potentials.[13] The latter explicitly includes Δ-degrees of freedom within a coupled-channel (CC) approach. Above pion threshold V_{28} is modified for the $^1D_2$ channel in order to give a better description of this channel as described in Ref. 14. For the other potential models we use the impulse approximation (IA) for the calculation of the IC.[14]

In the current operator we include explicit meson exchange contributions beyond the Siegert operators, essentially from π- and ρ-exchange, and isobar contributions. For the electromagnetic form factors of the one-body current we use two models: (i) the dipole fit with the two choices $G_{En}=0$, $G_{En}=D$ (with $p=5.6$) [15] for the neutron electric form factor and (ii) the Gari-Krümpelmann model (GK).[16] Finally, for the meson-exchange-current form factor we consider, in view of the unresolved controversial issue, both cases G_E^V and F_1^V.[17] In detail we will investigate the following effects: the influence of meson-exchange (MEC) and isobar currents (IC), the potential-model dependence, and neutron electric (G_{En}) and MEC form factor effects (G_E^V vs F_1^V).

The form factors $F_{\lambda\mu}^{(\prime)IM}$ are functions of E_{np} and $q^2_{\rm c.m.}$, the relative n-p energy and the three-momentum transfer squared, respectively, both in the c.m. system which cover a whole plane. Guided by the results of an earlier study[9] we have chosen three specific kinematical regions in the E_{np}-$q^2_{\rm c.m.}$ plane where the various above-mentioned effects show up in different ways:

(i) crossing the quasifree peak at a fixed momentum transfer ($q^2_{\rm c.m.}=12$ fm^{-2}), since for the quasifree kine-

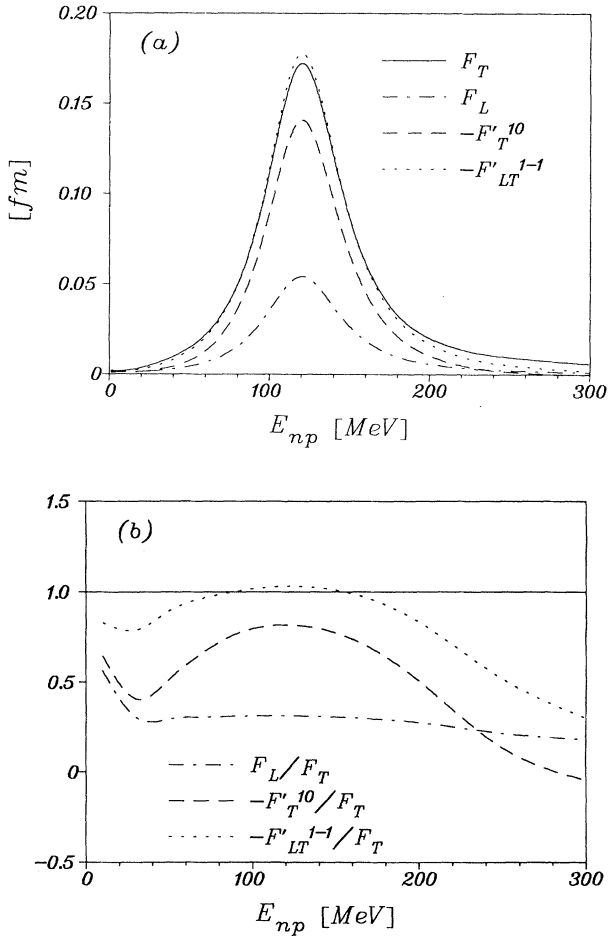

FIG. 2. The form factors F_T (full curve), F_L (dash-dotted curve), $F_T^{\prime 10}$ (dashed curve), and $F_{LT}^{\prime 1-1}$ (dotted curve) at $q^2_{\rm c.m.}=12$ fm^{-2} with the Paris potential, and $G_{En}=0$. (a) absolute magnitudes, (b) $F_L, F_T^{\prime 10}$, and $F_{LT}^{\prime 1-1}$ relative to F_T.

matics the influence of final-state interactions and interaction currents such as MEC and IC is minimal;

(ii) near the deuteron breakup threshold (E_{np} = 1.5 MeV), where one has a strong influence from π- and ρ-MEC and to a lesser extent from Δ-IC on the dominating transverse $M1$-matrix elements;

(iii) the Δ-resonance region (E_{np} =240 MeV), where the Δ-excitation and thus Δ-degrees of freedom play a very important, if not dominant, role.

Though the nonpolarization form factors F_L and F_T are already well studied in the literature, at least below pion threshold, we will include them in our discussion in order to have a scale for comparison of the various possible effects.

For the first kinematical region ($q^2_{\text{c.m.}}$=12 fm^{-2}) one may divide the eight form factors—here F^{1-1}_{LT} and F'^{2-1}_{LT} are not considered since they either vanish or are negligible—into two groups. Members of the first group ($F_L, F_T, F'^{1-1}_{LT}, F'^{10}_{T}$) have corresponding counterparts in electron scattering from a single nucleon $\vec{N}(\vec{e},e')N$ and should therefore exhibit a typical one-body response in the quasifree region. In other words, the scalar and vector form factors are dominated in the quasifree kinematics by the one-body process, while effects where the two-body density enters do not significantly contribute. The remaining tensor form factors (F^{20}_{L}, F^{20}_{T}, F^{2-1}_{LT}, F^{2-2}_{TT}) are not present in the single nucleon process. Their existence thus is intimately related to the presence of the other nucleon in order to form a spin $S = 1$ system necessary for a tensor polarization. This fact presumably leads to a different response, and, therefore, we expect in contrast to the one-body character of the scalar and vector form factors that the tensor form factors exhibit a larger sensitivity to the deuteron D state, to the final

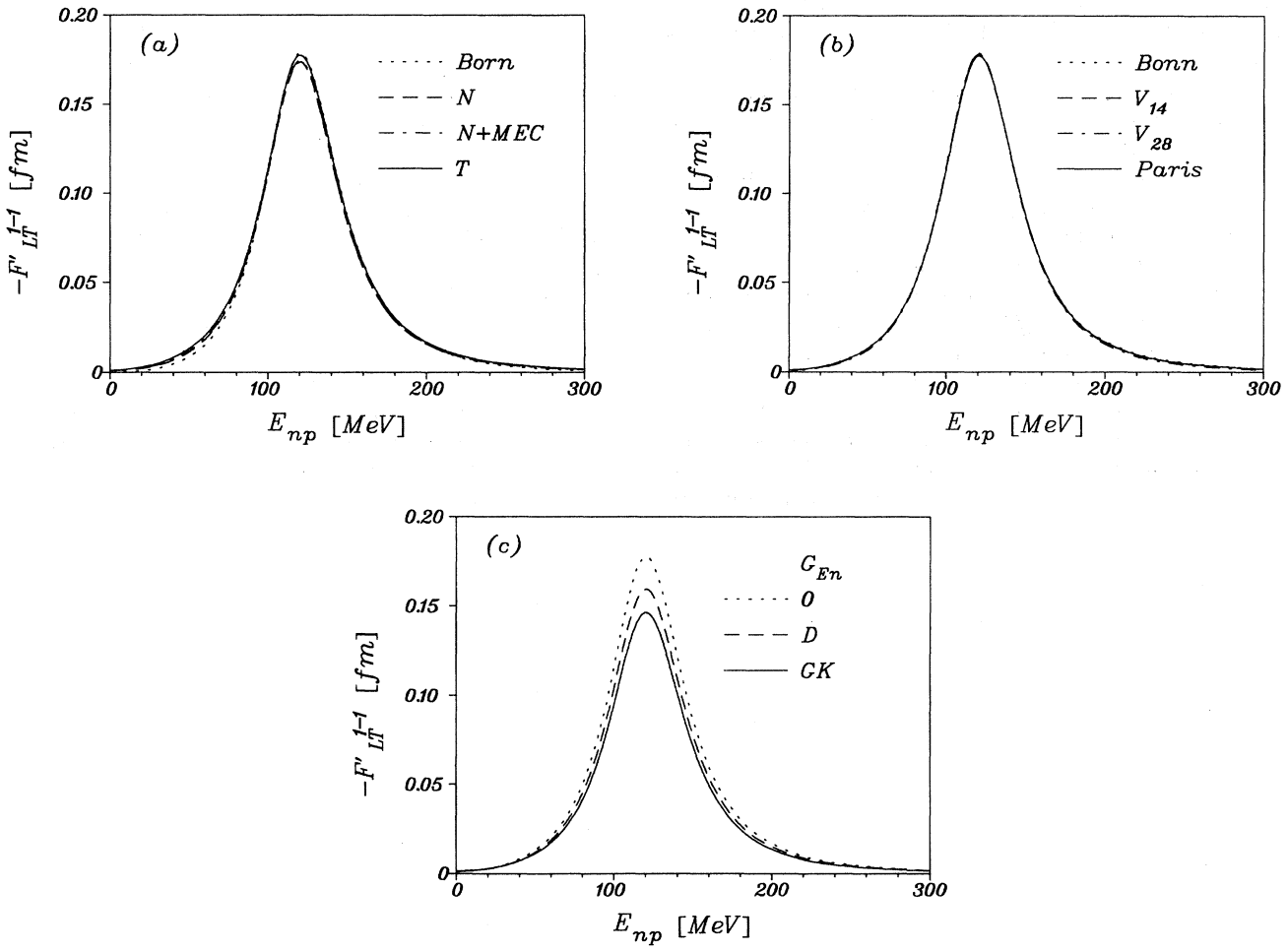

FIG. 3. The form factor F'^{1-1}_{LT} at $q^2_{\text{c.m.}}$ =12 fm^{-2}. (a) influence of final-state interaction and subnuclear degrees of freedom with Paris potential and G_{En} = 0: normal part (N) consisting of one-body currents plus Siegert operators with inclusion of final-state interaction (dashed curve), Born approximation (Born) as N but without final-state interaction (dotted curve), N with additional π MEC (N+MEC, dash-dotted curve) and further addition of IC (T, full curve). (b) potential model dependence (G_{En} = 0): Paris (full curve), V_{14} (dashed curve), Bonn (dotted curve) and V_{28} (dash-dotted curve) potential. (c) influence of G_{En} (Paris potential): G_{En} = 0 (dotted curve), G_{En} = D (dashed curve), and G_{En} = GK (full curve).

state interaction, and to MEC and IC.

Figure 2 shows the results for the first group. As expected they all have a peak in the quasifree region. The peak heights of F_T, F_T^{10}, and $F_{LT'}^{1-1}$ are rather similar, while that of F_L is about a factor of 3 smaller. The shapes of the curves of $F_T^{\prime 10}$ and $F_{LT'}^{\prime 1-1}$ are somewhat different from those of F_L and F_T as is evident from the lower part of Fig. 2. In particular, $F_T^{\prime 10}$ has a stronger fall-off on both sides of the peak.

Since all four form factors are affected in a rather similar way by MEC, IC, and final-state interactions, we will only discuss $F_{LT'}^{\prime 1-1}$ in detail. We choose this form factor, because it is the only one with a strong dependence on G_{En}. One readily sees this dependence in Fig. 3 where, for example, the maximum of the peak is reduced by 10% and 17% for the D and GK fits, respectively. These results are not surprising (see also Refs. 2, 4, and 5), since the relatively small G_{En} enters linearly in $F_{LT'}^{\prime 1-1}$ through interference with G_{Mn} and not quadratically as for the other three form factors of this group. On the contrary, MEC and IC have only negligible effects in the peak region, while in the tails their influence can become larger. Also the various potential models lead only to very small differences over the entire energy range considered. The tiny influence of subnuclear currents and the almost negligible potential model dependence are particularly interesting and encouraging with respect to the effects of the neutron electric form factor.

Therefore, we will investigate in addition the momentum dependence of this effect along the quasifree ridge, i.e., $E_{np}/\mathrm{MeV}=10\ q^2_{\mathrm{c.m.}}/\mathrm{fm}^{-2}$. However, for this purpose we prefer to directly discuss the asymmetry α_{ed}^V. The results in Fig. 4 show that even at lower momentum transfer G_{En} has a significant influence. Furthermore, increasing momentum transfer the effects become even more pronounced. Thus a determination of G_{En} seems to be quite possible. However, compared to the asymmetry A_{ed}^V of the exclusive process the uncertainties are larger due to the fact that α_{ed}^V does not vanish for $G_{En} = 0$. Thus a higher accuracy is required and the extraction of G_{En} from α_{ed}^V would have to rely heavier on a theoretical calculation. Since the dependences on potential models and on subnuclear degrees of freedom are small, the major theoretical uncertainties arise from relativistic effects which we have ignored completely in the present work and which might have a significant influence on the absolute value of α_{ed}^V. Assuming that relativistic effects are similar in size for the two form factors $F_{LT'}^{\prime 1-1}$ and $F_T^{\prime 10}$ one could use the latter one to check their importance by studying $\alpha_{ed}^V(0,0)$, since in this case only $F_T^{\prime 10}$, which is almost not affected by G_{En}, contributes to α_{ed}^V.

Now we turn to the second group of form factors (F_L^{20}, F_T^{20}, F_{LT}^{2-1}, F_{TT}^{2-2}). Figure 5 shows that they are rather small and that they all exhibit an interference pattern instead of having the typical quasifree peak structure. Their different behavior is also illustrated in Fig. 6, where one readily notes a sizeable influence from the final state interaction even at quasifree kinematics for F_T^{20}, F_{LT}^{2-1}, and F_{TT}^{2-2}. Only F_L^{20} is not shown because the effects are small. In one case (F_{LT}^{2-1}) it even leads to a complete sign change. Furthermore, these form factors are also quite strongly influenced by MEC and IC. Isobar effects are particularly large for F_{TT}^{2-2}. The size of the potential model dependence is rather similar for all four form factors and for this reason we only show it for F_{LT}^{2-1} and F_{TT}^{2-2} in Fig. 7. It is evident that there is only a moderate influence from the potential model.

We would like to point out a specific sensitivity of F_L^{20} to the deuteron D wave. In fact, it is easy to show using the explicit expressions in Ref. 3 that for a pure S-wave deuteron F_L^{20} vanishes identically in Born approximation. Final-state interaction and subnuclear degrees of freedom do not change this result significantly. This is demonstrated in Table I, where we list for quasifree kinematics

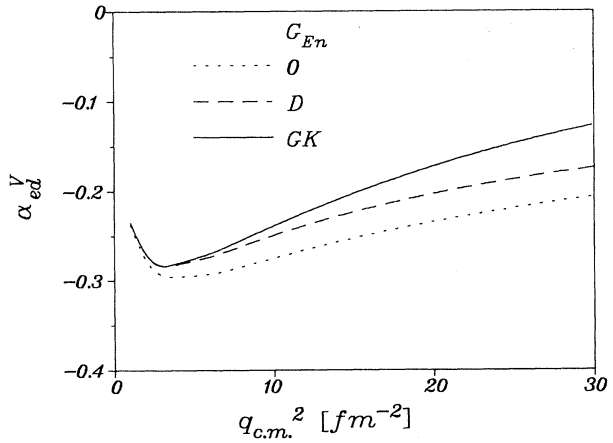

FIG. 4. Influence of G_{En} on the beam-vector-target asymmetry $\alpha_{ed}^V(\frac{\pi}{2}, 0)$ (Paris potential, quasifree kinematics with $\theta_e = 60°$). Notation as in Fig. 3(c).

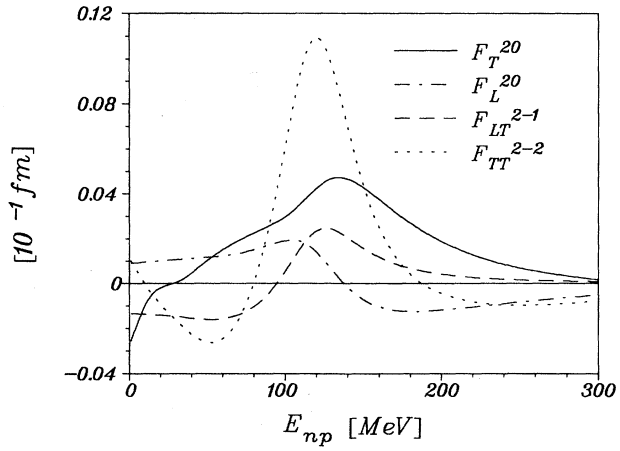

FIG. 5. The form factors F_T^{20} (dotted curve), F_L^{20} (dashed curve), F_{LT}^{2-1} (dash-dotted curve), and F_{TT}^{2-2} (full curve) at $q^2_{\mathrm{c.m.}} = 12\ \mathrm{fm}^{-2}$ (Paris potential, $G_{En} = 0$).

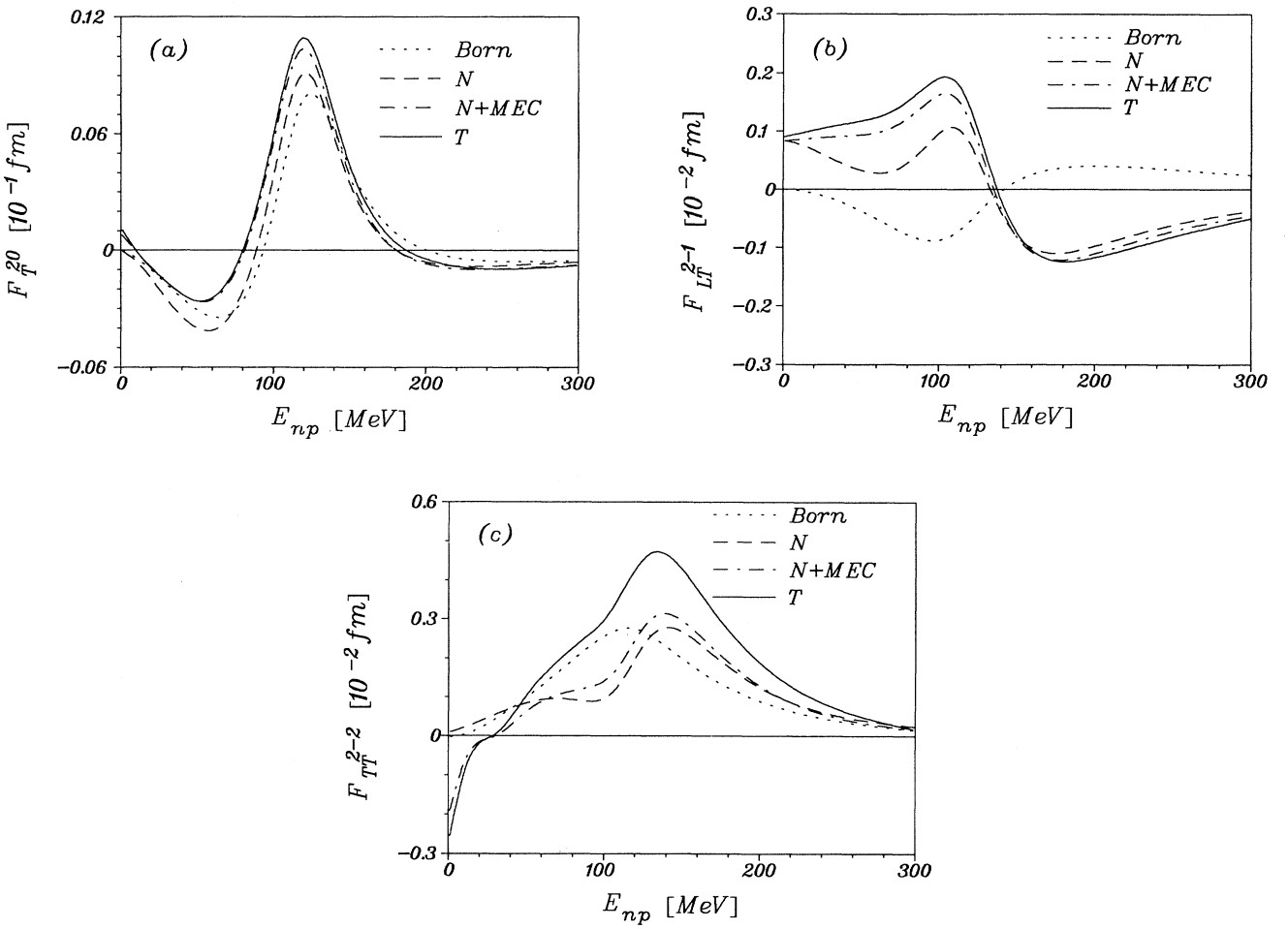

FIG. 6. Various contributions from final state interaction and subnuclear degrees of freedom to the form factors F_T^{20} (a), F_{LT}^{2-1} (b), and F_{TT}^{2-2} (c) at $q^2_{\text{c.m.}}$ =12 fm^{-2} (Paris potential, $G_{En}=0$). Notation as in Fig. 3(a).

the results for F_L^{20} with and without the D wave. One notes for $T = N$+MEC+IC a reduction by almost an order of magnitude if the D wave is switched off. In order to see whether this sensitivity allows one to investigate the D wave in greater detail, we have studied F_L^{20} along the quasifree ridge. However, the differences between different potential models are small and, moreover, final-state-interaction effects are sizeable. Therefore, despite its sensitivity to the D wave, F_L^{20} is not suited for a study of the deuteron D wave. Finally, with respect to the neutron electric form factor only F_L^{20} and F_{LT}^{2-1} are significantly affected as can be seen in Fig. 8 for F_{LT}^{2-1}.

Deuteron breakup near threshold is the classical region for the study of MEC in electron scattering. In this case it is not sufficient to use only the π MEC consistent with the potential model because also the ρ MEC leads to important contributions here. Other exchange currents which in principle are required for consistency can safely be neglected because their effect remains small.[18] For the Paris and Bonn potentials we take the π and ρ parametrization consistent with the corresponding potential, while for the phenomenological Argonne potentials we use the following parameters: Λ_π =5 fm^{-1} (monopole), $g^2_{NN\rho}/4\pi = 0.95$, $f_{NN\rho}/g_{NN\rho} = 6.1$, and Λ_ρ =1.3 GeV (dipole).

According to the importance of the MEC contribution we again divide the eight form factors into two groups. The first group (F_T, F_T^{20}, F_{TT}^{2-2}, $F_T'^{10}$) contains all the form factors where the MEC dominated $M1$ transition to the $^1S_0$ quasi-bound state contributes. If one had only this transition, one would obtain from (A2), (A5), (A9), and (A10) of the Appendix the following simple relations

$$F_T'^{10} = -\sqrt{\tfrac{3}{2}}F_T, \quad F_T^{20} = \frac{1}{\sqrt{2}}F_T, \quad F_{TT}^{2-2} = -\sqrt{3}F_T \ . \tag{35}$$

Figure 9 shows that the above relations are approximately fulfilled, thereby underlining the dominance of this transition. Of course, these relations are no longer

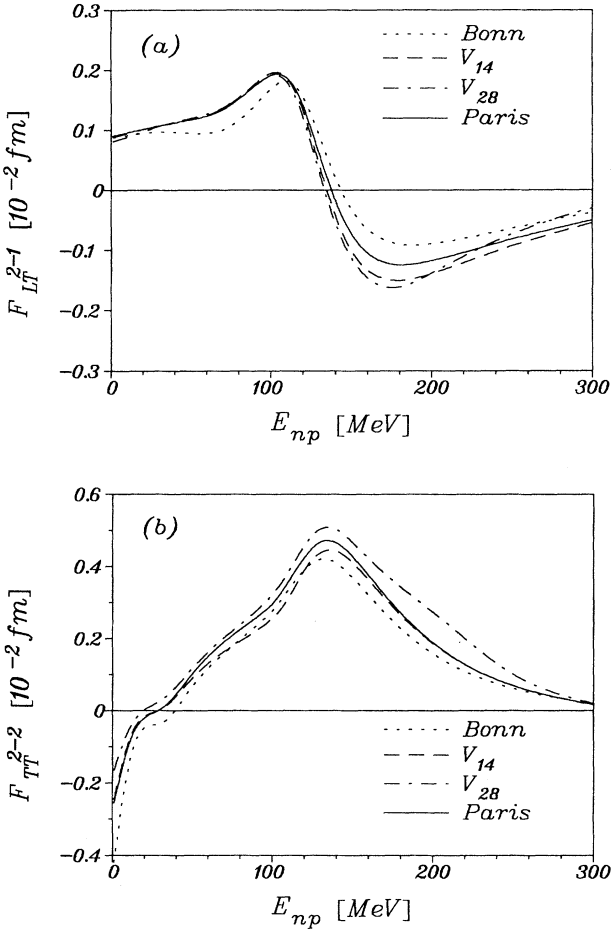

FIG. 7. Potential-model dependence for the form factors F_{LT}^{2-1} (a) and F_{TT}^{2-2} (b) at $q^2_{\text{c.m.}}$ =12 fm^{-2} ($G_{En}=0$). Notation as in Fig. 3(b).

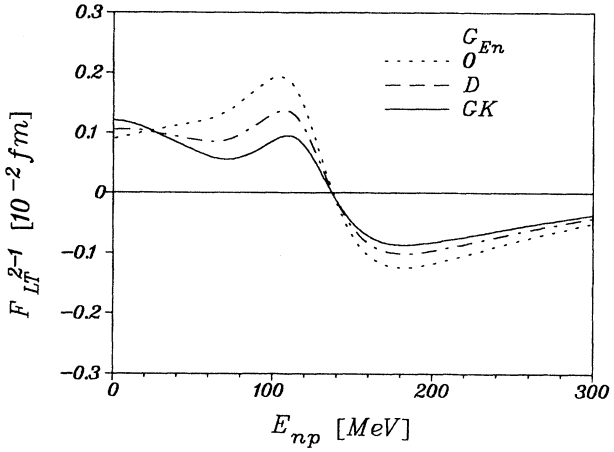

FIG. 8. Influence of G_{En} on the form factor F_{LT}^{2-1} at $q^2_{\text{c.m.}}$ =12 fm^{-2} (Paris potential). Notation as in Fig. 3(c).

valid in the region of the minima because here transitions to other partial waves of the final state become important.

In view of the similar behavior of these form factors, apart from the minimum region, it is sufficient to discuss in the following only one of the four form factors, e.g., $F_T'^{10}$. The crucial role of MEC becomes evident in Fig. 10. One notes that the strong MEC contribution shifts the minimum of the normal part N to a much higher momentum transfer. With respect to the potential model dependence, the very different behavior if one uses the Bonn potential is most evident. For F_T this fact has already been discussed in Ref. 19, where we have pointed out that this different behavior cannot solely be attributed to a lower D-state admixture in the deuteron. Another strong effect of similar size originates from the choice of the MEC form factor, i.e., whether one uses F_1^V or G_E^V. This latter effect also depends very much on the model for G_{En}.[17]

The four remaining form factors ($F_L, F_L^{20}, F_{LT}^{2-1}, F_{LT}'^{1-1}$) are shown together in Fig 11. With increasing momentum transfer they all fall off rather rapidly. F_L exhibits the weakest and $F_{LT}'^{1-1}$ the strongest slope. For the purely longitudinal form factors F_L and F_L^{20} there are of course no MEC contributions. However, even for the two LT interference form factors one finds only a tiny influence from MEC. This is explained by the fact that the lead-

TABLE I. The longitudinal tensor form factor F_L^{20} at E_{np} = 120 MeV and $q^2_{\text{c.m.}}$ =12 fm^{-2} with and without D wave in 10^{-3} fm.

D wave	N	T	Born
Yes	2.33	2.36	2.42
No	−0.319	−0.315	0.0

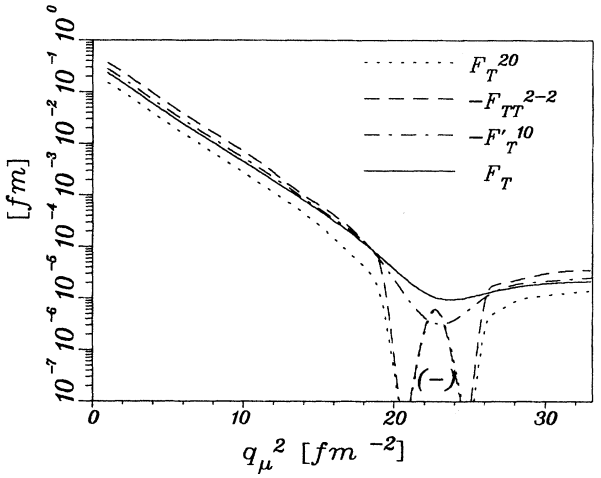

FIG. 9. The form factors F_T^{20} (dotted curve), F_{TT}^{2-2} (dashed curve), $F_T'^{10}$ (dash-dotted curve), and F_T (full curve) at E_{np} =1.5 MeV (Paris potential, $G_{En}=0$).

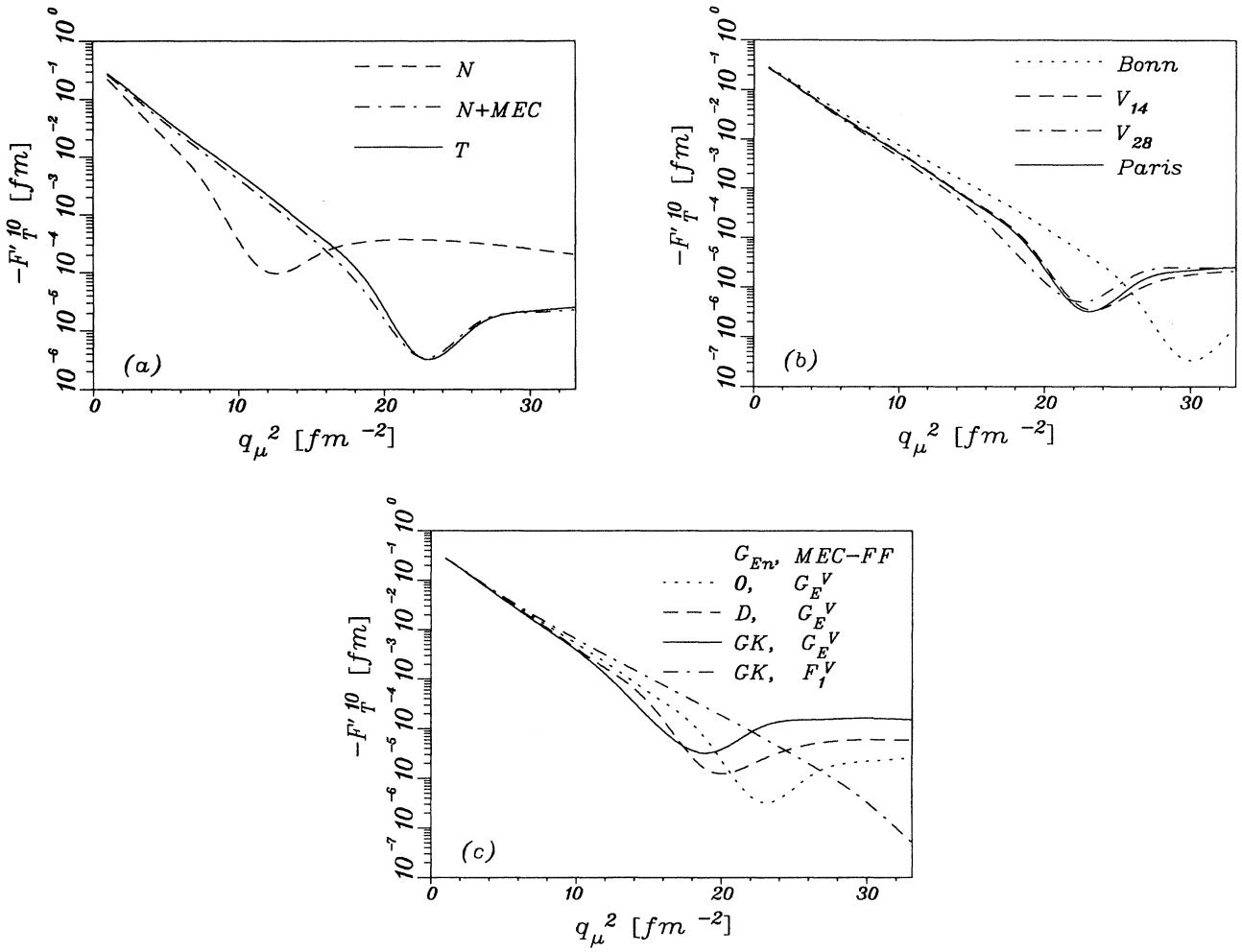

FIG. 10. The form factor $F_T'^{10}$ at E_{np} =1.5 MeV. (a) and (b) as corresponding parts of Fig. 3, but MEC contribution in (b) includes also ρ MEC. (c) dependence on G_{En} and MEC form factors: G_E^V as MEC form factor with $G_{En} = 0$ (dotted curve), with $G_{En} = D$ (dashed curve), and with $G_{En} = GK$ (full curve) and F_1^V as MEC form factor with $G_{En} = GK$ (dash-dotted curve).

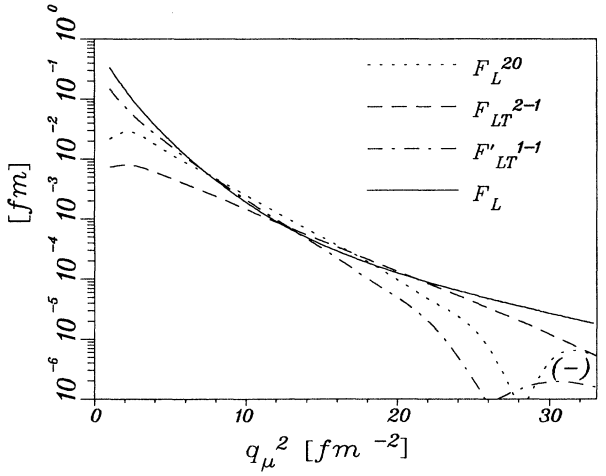

FIG. 11. The form factors F_L^{20} (dotted curve), F_{LT}^{2-1} (dashed curve), $F_{LT}'^{1-1}$ (dash-dotted curve), and F_L (full curve) at E_{np} = 1.5 MeV (Paris potential, G_{En} = 0). A sign change is indicated by (−).

ing LT interference originates from the $C0, C2$, and $M1$ multipoles of the transition to the coupled $^3S_1$-$^3D_1$ state. Since this is an isoscalar transition, the dominant isovector MEC do not contribute even for $M1$. We should mention that there is no interference of the strongly MEC influenced $M1$ transition to the $^1S_0$ state as there is no Coulomb transition to this state.

Since all four form factors are influenced similarly in size by the various effects we are considering here, we only discuss F_L^{20} in more detail. Figure 12 shows that there is only a small IC contribution and, furthermore, that differences due to the various potential models also remain small. The effect of G_{En} is a little more sizeable. However, apart from the uncertainty due to unknown relativistic effects, one would not base a determination of G_{En} on a measurement of this quantity since the analysis would be marred by the potential model dependence and IC contribution which are almost of the same size than the influence of G_{En}.

For the third kinematical region, the Δ-resonance re-

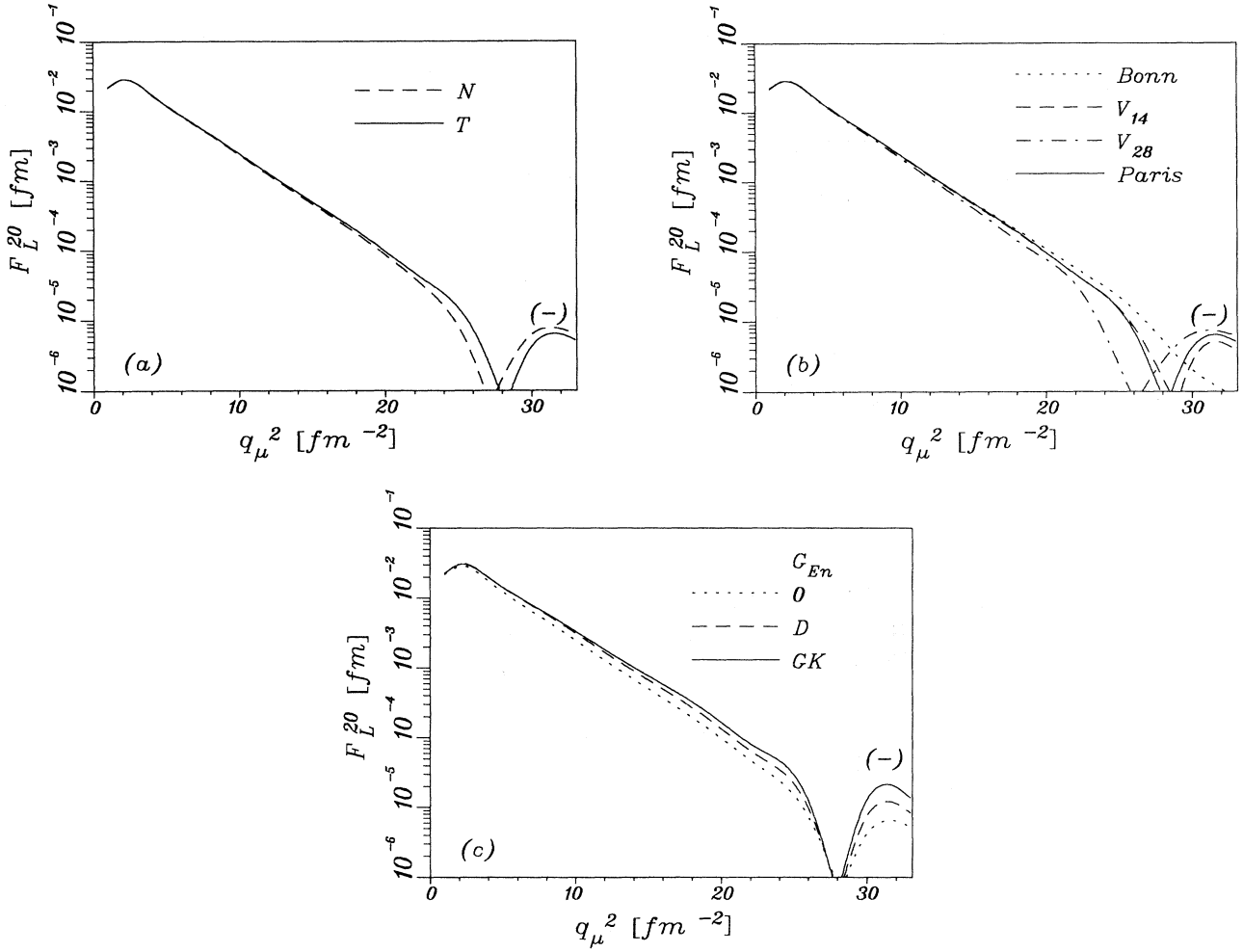

FIG. 12. The form factor F_L^{20} at $E_{np} = 1.5$ MeV. Notations as in Fig. 3. A sign change is indicated by (−).

gion, we divide the form factors into three subgroups. The first two groups are identical with the two groups of the second kinematics, while the third group consists of the additional two form factors F_{LT}^{1-1} and $F_{LT}^{\prime 2-1}$. As mentioned previously these vanish below pion threshold, but might become important in the Δ-resonance region. The reason for the separation of the first two groups is again an $M1$ transition, but in this case to the $^1D_2$ partial wave. This transition is most strongly affected by IC contributions, since only in this case there is a coupling of an $N\Delta$-partial wave in a relative S state ($^5S_2$) to the NN configuration. We will show the various form factors at a fixed energy $E_{np} = 240$ MeV but for varying momentum transfer ranging from the photon point, i.e., $q^2_{\text{c.m.}} = 1.34$ fm^{-2}, up to $q^2_{\text{c.m.}} = 20$ fm^{-2}. The upper limit is already quite close to the quasifree peak which is located at $q^2_{\text{c.m.}} = 24$ fm^{-2}.

Figure 13 shows the results for the various form factors of the first group. F_T and $F_T^{\prime 10}$ are similar in size, while F_T^{20} and F_{TT}^{2-2} are about one order of magnitude smaller.

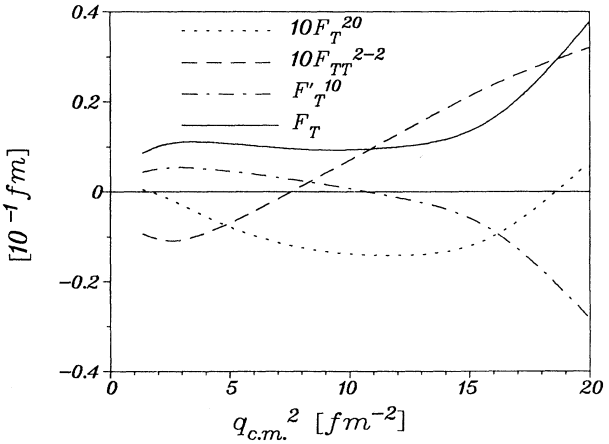

FIG. 13. The form factors F_T^{20} (dotted curve), F_{TT}^{2-2} (dashed curve), $F_T^{\prime 10}$ (dash-dotted curve), and F_T (full curve) at $E_{np} = 240$ MeV (CC with V_{28} potential, $G_{En} = 0$). Note that the curves for F_T^{20} and F_{TT}^{2-2} are multiplied by a factor of 10.

They all increase towards higher momentum transfer as the quasifree peak is approached (see Fig. 2). The contributions of MEC and IC are shown in Fig. 14. One finds for the two stronger form factors (F_T, $F_T'^{10}$) the largest IC effects at lower momentum transfer, e.g., at $q^2_{\text{c.m.}} = 2$ fm^{-2} where one has an increase from IC by a factor of 3.3 for F_T and by 5.1 for $F_T'^{10}$. The large influence from IC makes $F_T'^{10}$ particularly interesting for the study of Δ degrees of freedom.

The other two form factors, though much smaller, also exhibit strong IC effects, which for these two cases are not restricted to the lower-momentum-transfer region. The potential-model dependence of F_T and $F_T'^{10}$ is rather unimportant, even if one compares the CC calculation using V_{28} with the IA of the other potential models. Therefore, we only show the potential influence for one of them ($F_T'^{10}$) in Fig. 15. But this might change if one moves away from the Δ peak according to what one finds in the photodisintegration of the deuteron in the Δ region,[14] where the CC results show a considerable sensitivity on the $N\Delta$ interaction. Compared to F_T^{20} and F_{TT}^{2-2} we find that F_T^{20} and F_{TT}^{2-2}—also shown in Fig. 15—are quite sensitive to the method by which Δ degrees of freedom are incorporated, i.e., IA or CC. The CC calculation leads to significantly different results underlining the importance of a proper treatment of Δ degrees of freedom for these two form factors.

The second group of form factors is depicted in Fig. 16. While F_L and $F_{LT}'^{1-1}$ are similar in size one finds that F_{LT}^{2-1} and F_L^{20} are respectively about one and two orders of magnitude smaller. Figure 17 shows the effects of subnuclear currents only on F_L^{20} and F_{LT}^{2-1}, because the other two form factors are not significantly affected. The IC contribution increases F_L^{20} by about a factor of 2 at lower momentum transfer, while F_{LT}^{2-1} is similarly influenced at somewhat higher momentum transfers. In

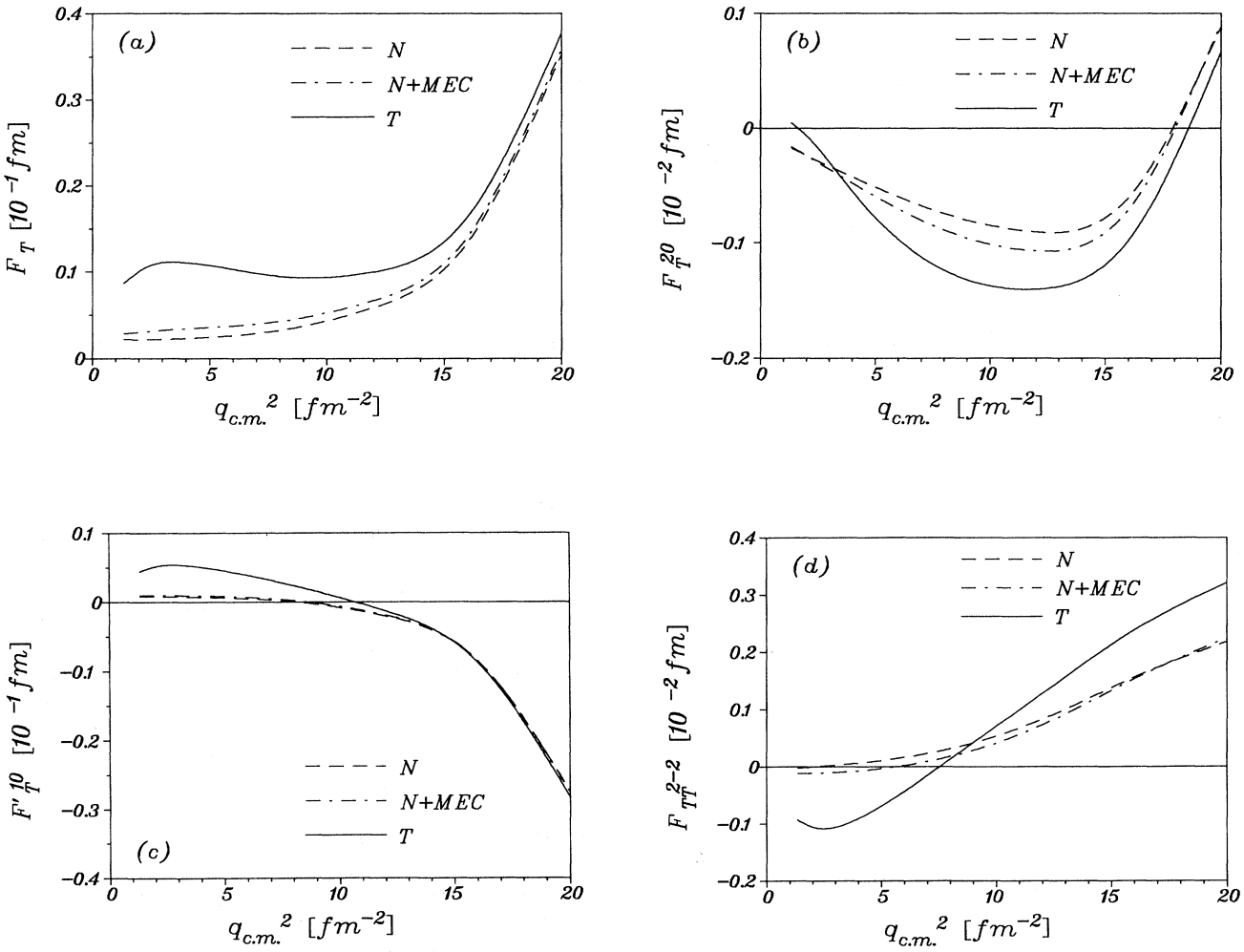

FIG. 14. Various contributions to the form factors F_T (a), F_T^{20} (b), $F_T'^{10}$ (c), and F_{TT}^{2-2} (d) at $E_{np} = 240$ MeV (CC with V_{28} potential, $G_{En} = 0$). Notation as in Fig. 3(a).

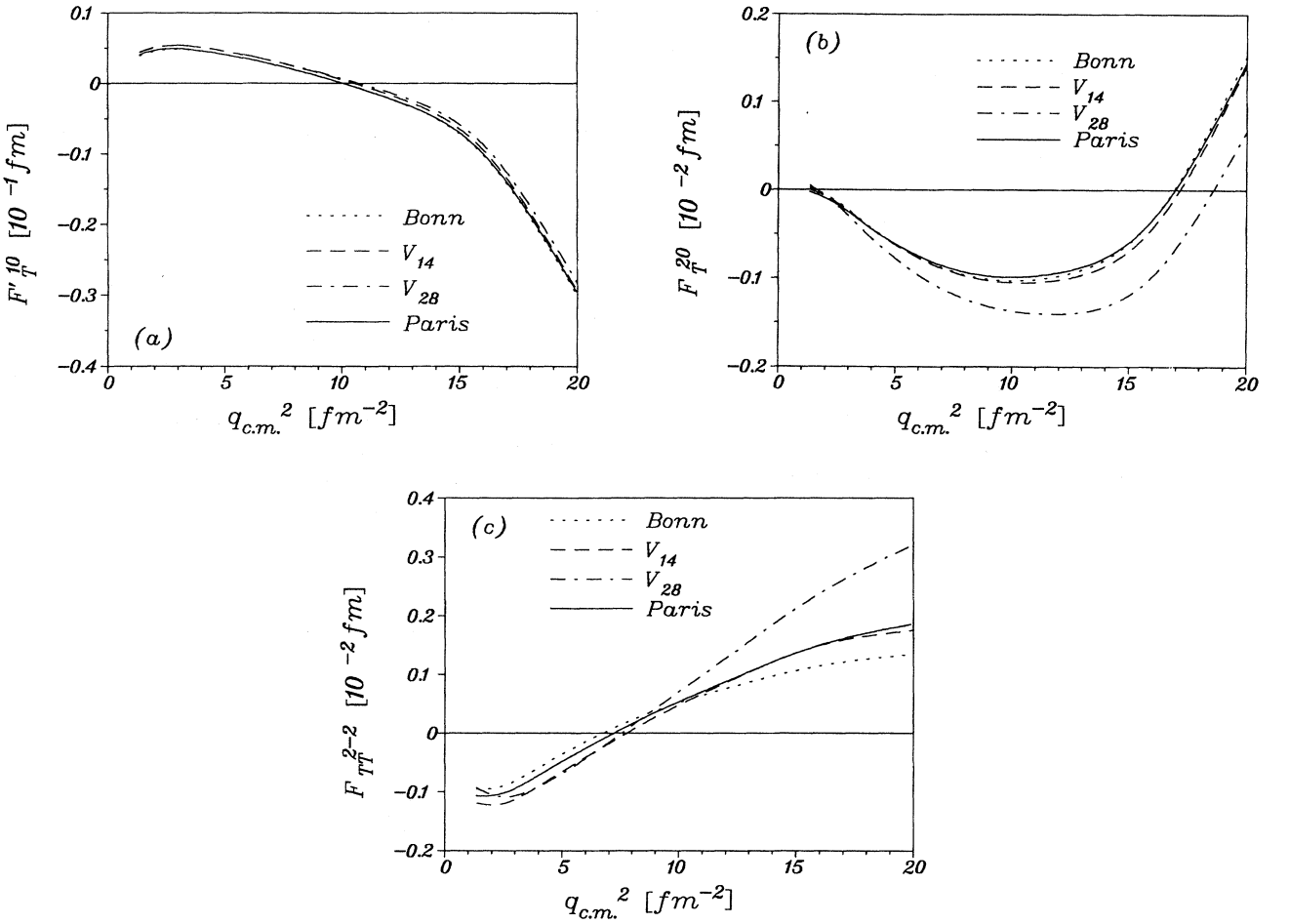

FIG. 15. Potential-model dependence for the form factors F'^{10}_T (a), F^{20}_T (b), and F^{2-2}_{TT} (c) at E_{np} =240 MeV ($G_{En} = 0$). Notation as in Fig. 3(b).

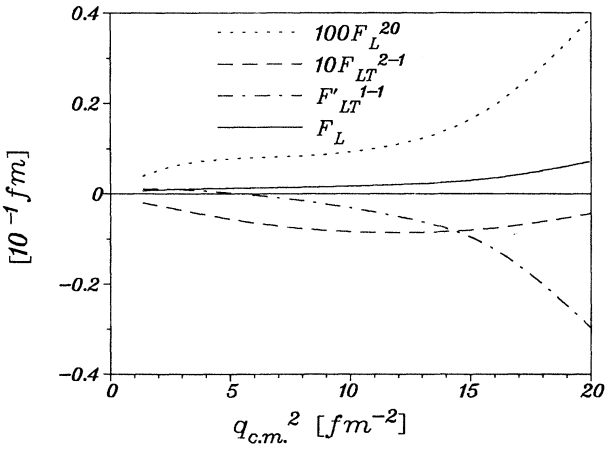

FIG. 16. The form factors F^{20}_L (dotted curve), F^{2-1}_{LT} (dashed curve), F'^{1-1}_{LT} (dash-dotted curve), and F_L (full curve) at $E_{np} = 240$ MeV (CC with V_{28} potential, $G_{En} = 0$). Note that the curves for F^{20}_L and F^{2-1}_{LT} are multiplied by factors of 100 and 10, respectively.

addition, F^{2-1}_{LT} has a rather strong MEC contribution.

The potential-model dependence is shown in Fig. 18. Only F'^{1-1}_{LT} is not shown, since the interesting effects are small. Comparing the results for V_{14} and V_{28}, one notes a rather strong effect leading to a reduction in size from the CC treatment at lower momentum transfer which is particularly interesting in the case of F_L. Though the direct IC contribution is very small, F_L is considerable reduced in the CC calculation with V_{28}, which is an indirect feedback effect of the IC channels on the NN channels. The other three potential models lead to almost identical results. A similar reduction is found for the normal contribution in deuteron photodisintegration in the Δ region from a CC treatment.[14] Compared to F_L the potential effects on F^{20}_L and F^{2-1}_{LT} are notably different. Besides the sizeable influence of the CC treatment, one notes in addition strong differences among the results of the other three potential models. We close the discussion with Fig. 19, which shows the form factors F^{1-1}_{LT} and F'^{2-1}_{LT}. Since they originate from the inelasticity due to

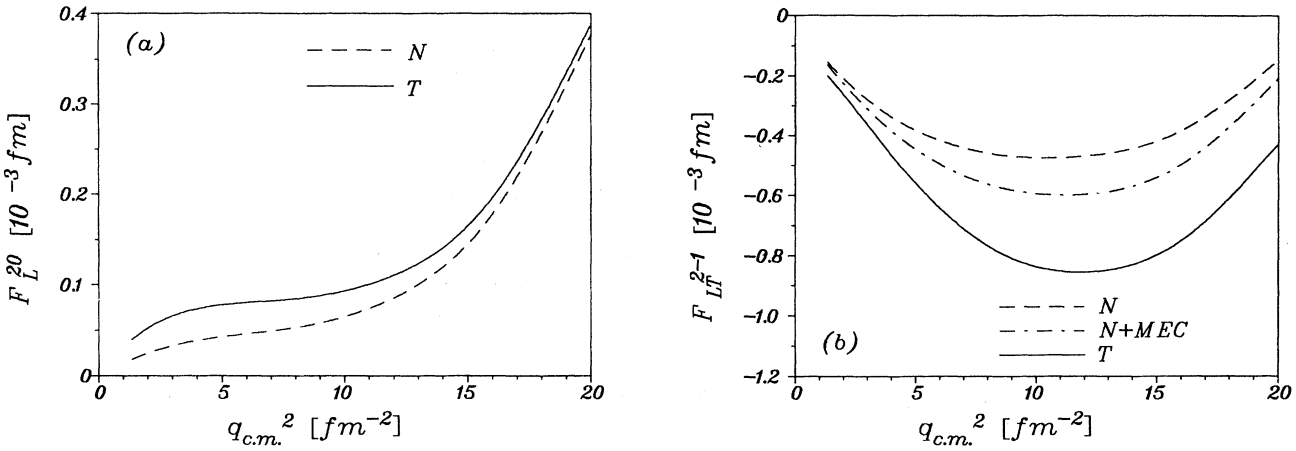

FIG. 17. Various contributions to the form factors F_L^{20} (a) and F_{LT}^{2-1} (b) at $E_{np} = 240$ MeV (CC with V_{28} potential, $G_{En} = 0$). Notation as in Fig. 3(a).

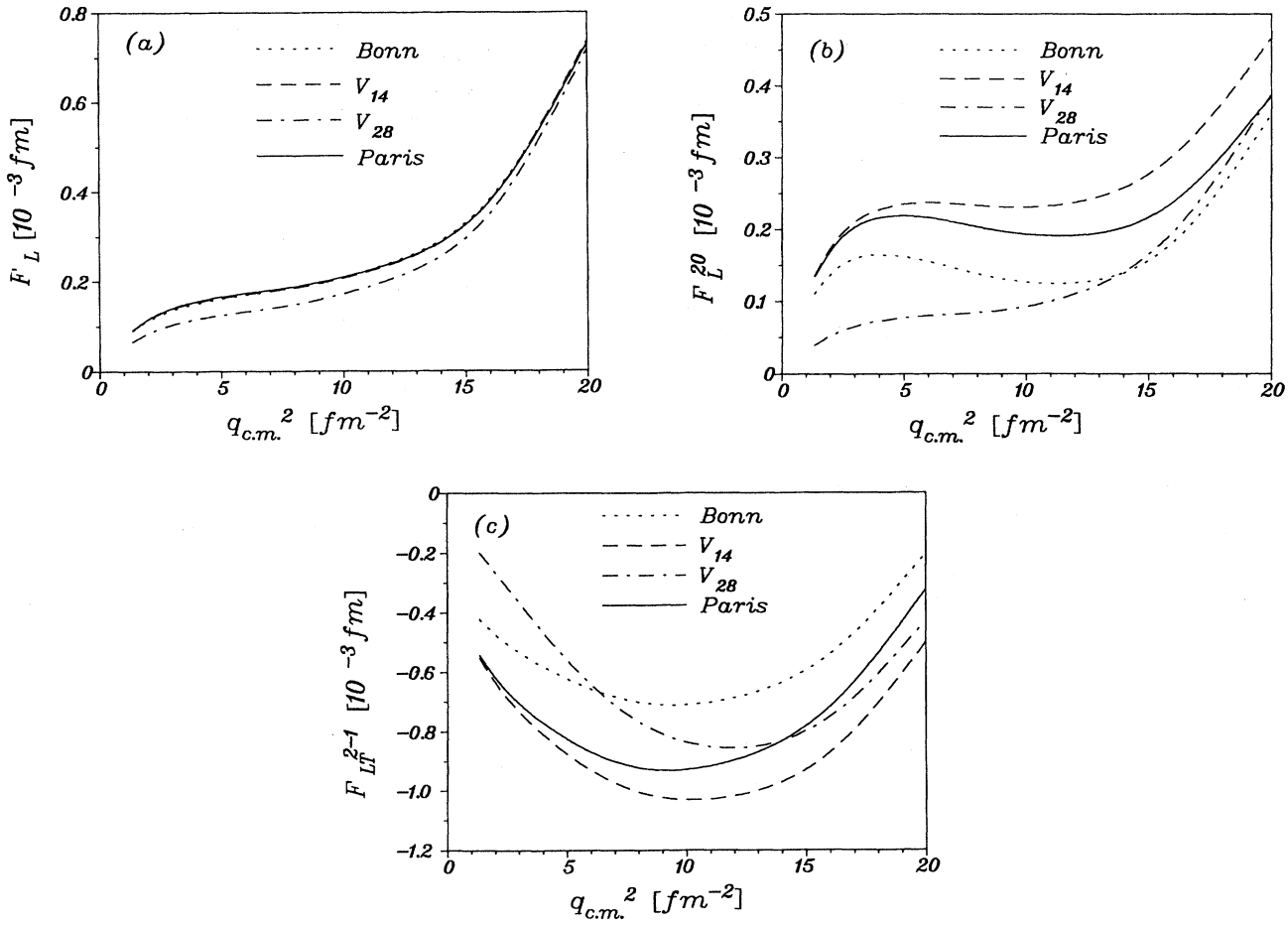

FIG. 18. Potential-model dependence for the form factors F_L (a), F_L^{20} (b), and F_{LT}^{2-1} (c) at $E_{np} = 240$ MeV ($G_{En} = 0$). Notation as in Fig. 3(b).

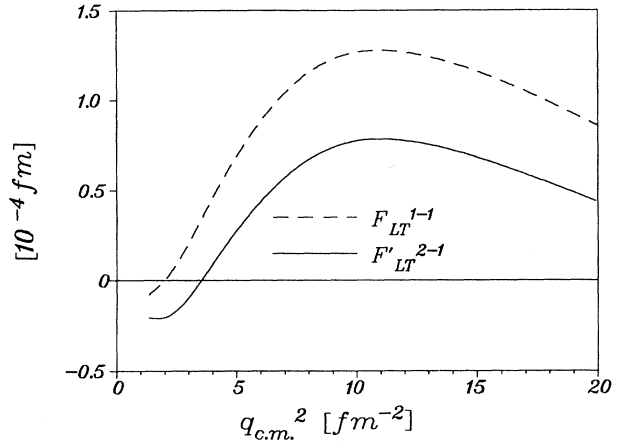

FIG. 19. The form factors F_{LT}^{1-1} (dashed curve) and $F_{LT}^{\prime 2-1}$ (full curve) at $E_{np} = 240$ MeV (CC with V_{28} potential, $G_{En} = 0$) .

the Δ dynamics, we only show the results for the CC calculation. However, they are both quite small compared with the various other form factors, so that Δ effects are much more pronounced in some of the other form factors.

Finally, we would like to summarize the most important results of our study. We have shown that the $^2\vec{\mathrm{H}}(\vec{e},e')np$ cross section depends on ten—below pion threshold eight—form factors, and each of these form factors can be separated experimentally. With respect to Δ degrees of freedom we find various interesting aspects. The form factors $F_T, F_T^{\prime 10}, F_T^{20}$, and F_{TT}^{2-2} all exhibit quite considerable IC contributions in the Δ-resonance region at lower momentum transfer of which $F_T^{\prime 10}$ shows the comparatively strongest influence for this kinematics. The two transverse tensor form factors F_T^{20} and F_{TT}^{2-2} are also affected in other kinematic regions. The latter one even shows rather strong IC contributions for quasifree kinematics. However, these two form factors are about an order of magnitude smaller than F_T and $F_T^{\prime 10}$. Furthermore, also the purely longitudinal and the longitudinal-transverse interference form factors show influences from Δ degrees of freedom. We only mention here F_L, F_L^{20}, and F_{LT}^{2-1}, which show notably different results if one compares the IA with the CC calculation. This is particularly interesting for F_L, since on the one hand IC contributions are negligible and on the other hand differences among potential models without explicit Δ degrees of freedom remain small. As regards the MEC we do not find such a variety of effects as due to the Δ resonance. The strongest MEC influences are present at the deuteron breakup threshold. Because of the dominance of the $M1$ transition to the $^1S_0$ partial wave $F_T^{\prime 10}, F_T^{20}$, and F_{TT}^{2-2} are very similarly affected as is the well-known F_T. One further interesting result is the rather strong dependence on the neutron electric form factor of $F_{LT}^{\prime 1-1}$ in the quasifree region, while at the same time potential and interaction current effects remain negligibly small. Thus the inclusive reaction $^2\vec{\mathrm{H}}(\vec{e},e')$ with a vector polarized deuteron target could be an interesting alternative to the more involved exclusive processes $^2\vec{\mathrm{H}}(\vec{e},e'n)p$ or $^2\mathrm{H}(\vec{e},e'\vec{n})$.

ACKNOWLEDGMENTS

This work was supported in part by the Deutsche Forschungsgemeinschaft (SFB 201) and in part by the Natural Sciences and Engineering Research Council of Cananda. Two of the authors (H.A. and W.L.) would like to thank the Saskatchewan Accelerator Laboratory for the hospitality extended to them during a visit. H.A. thanks J. van den Brand for an interesting discussion concerning the role of the D wave in the tensor form factors.

APPENDIX A

Here we will list the explicit expressions for the multipole decomposition of the various form factors.

The unpolarized form factors are given by

$$F_L = \frac{16\pi^2}{3}\sum_{Lj\lambda}\frac{1}{2L+1}|C^L(\lambda j)|^2, \tag{A1}$$

$$F_T = \frac{16\pi^2}{3}\sum_{Lj\lambda}\frac{1}{2L+1}[|E^L(\lambda j)|^2 + |M^L(\lambda j)|^2]. \tag{A2}$$

The vector polarization form factors are given by

$$F_{LT}^{1-1} = -32\pi^2\sqrt{2}\sum_{LL'j\lambda}(-)^j \begin{pmatrix} L' & L & 1 \\ 0 & -1 & 1 \end{pmatrix}\begin{Bmatrix} L' & L & 1 \\ 1 & 1 & j \end{Bmatrix}\mathrm{Im}\{C^{L'}(\lambda j)^*[E^L(\lambda j) + M^L(\lambda j)]\}, \tag{A3}$$

$$F_{LT}^{\prime 1-1} = 32\pi^2\sqrt{2}\sum_{LL'j\lambda}(-)^j \begin{pmatrix} L' & L & 1 \\ 0 & -1 & 1 \end{pmatrix}\begin{Bmatrix} L' & L & 1 \\ 1 & 1 & j \end{Bmatrix}\mathrm{Re}\{C^{L'}(\lambda j)^*[E^L(\lambda j) + M^L(\lambda j)]\}, \tag{A4}$$

$$F_T^{\prime 10} = 16\pi^2\sum_{LL'j\lambda}(-)^j \begin{pmatrix} L' & L & 1 \\ 1 & -1 & 0 \end{pmatrix}\begin{Bmatrix} L' & L & 1 \\ 1 & 1 & j \end{Bmatrix}\mathrm{Re}[[E^{L'}(\lambda j) + M^{L'}(\lambda j)]^*[E^L(\lambda j) + M^L(\lambda j)]]. \tag{A5}$$

Finally, the tensor polarization form factors

$$F_L^{20} = -16\pi^2\sqrt{\tfrac{5}{3}}\sum_{LL'j\lambda}(-)^j \begin{pmatrix} L' & L & 2 \\ 0 & 0 & 0 \end{pmatrix} \begin{Bmatrix} L' & L & 2 \\ 1 & 1 & j \end{Bmatrix} \mathrm{Re}[C^{L'}(\lambda j)^* C^L(\lambda j)], \tag{A6}$$

$$F_{LT}^{2-1} = 32\pi^2\sqrt{\tfrac{10}{3}}\sum_{LL'j\lambda}(-)^j \begin{pmatrix} L' & L & 2 \\ 0 & -1 & 1 \end{pmatrix} \begin{Bmatrix} L' & L & 2 \\ 1 & 1 & j \end{Bmatrix} \mathrm{Re}\{C^{L'}(\lambda j)^*[E^L(\lambda j) + M^L(\lambda j)]\}, \tag{A7}$$

$$F_{LT}'^{2-1} = -32\pi^2\sqrt{\tfrac{10}{3}}\sum_{LL'j\lambda}(-)^j \begin{pmatrix} L' & L & 2 \\ 0 & -1 & 1 \end{pmatrix} \begin{Bmatrix} L' & L & 2 \\ 1 & 1 & j \end{Bmatrix} \mathrm{Im}\{C^{L'}(\lambda j)^*[E^L(\lambda j) + M^L(\lambda j)]\}, \tag{A8}$$

$$F_T^{20} = 16\pi^2\sqrt{\tfrac{5}{3}}\sum_{LL'j\lambda}(-)^j \begin{pmatrix} L' & L & 2 \\ 1 & -1 & 0 \end{pmatrix} \begin{Bmatrix} L' & L & 2 \\ 1 & 1 & j \end{Bmatrix} \mathrm{Re}\{[E^{L'}(\lambda j) + M^{L'}(\lambda j)]^*[E^L(\lambda j) + M^L(\lambda j)]\}, \tag{A9}$$

$$F_{TT}^{2-2} = 16\pi^2\sqrt{\tfrac{5}{3}}\sum_{LL'j\lambda}(-)^j \begin{pmatrix} L' & L & 2 \\ -1 & -1 & 2 \end{pmatrix} \begin{Bmatrix} L' & L & 2 \\ 1 & 1 & j \end{Bmatrix} \mathrm{Re}\{[E^{L'}(\lambda j) - M^{L'}(\lambda j)]^*[E^L(\lambda j) + M^L(\lambda j)]\}. \tag{A10}$$

[1] C.Y. Cheung and R.M. Woloshyn, Phys. Lett. **127B**, 147 (1983).

[2] B. Blankleider and R.M. Woloshyn, Phys. Rev. C **29**, 538 (1983).

[3] H. Arenhövel, W. Leidemann, and E.L. Tomusiak, Z. Phys. A **331**, 123 (1988); **334**, 363(E) (1989).

[4] M.P. Rekalo, G.I. Gakh, and A.P. Rekalo, J. Phys. G **13**, 1209 (1987); Phys. Lett. B **205**, 432 (1988).

[5] W. Leidemann, E. Lipparini, and S. Stringari, Phys. Rev. C **42**, 416 (1990).

[6] T.W. Donnelly and A.S. Raskin, Ann. Phys. (N.Y.) **169**, 247 (1986).

[7] V. Dmitrasinovic and F. Gross, Phys. Rev. C **40**, 2479 (1989).

[8] B.A. Robson, *The Theory of Polarization Phenomena* (Clarendon Press, Oxford, 1974).

[9] W. Fabian and H. Arenhövel, Nucl. Phys. **A314**, 253 (1979).

[10] H. Arenhövel and M. Sanzone, Few-Body Syst., Suppl. (in press).

[11] M. Lacombe, B. Loiseau, J.M. Richard, R. Vinh Mau, J. Côté, P. Pirès, and R. de Tourreil, Phys. Rev. C **21**, 861 (1980).

[12] R. Machleidt, K. Holinde, and Ch. Elster, Phys. Rep. **149**, 1 (1987).

[13] R.W. Wiringa, R. Smith, and T.L. Ainsworth, Phys. Rev. C **29**, 1207 (1984).

[14] W. Leidemann and H. Arenhövel, Nucl. Phys. **A465**, 573 (1987); P. Wilhelm, W. Leidemann, and H. Arenhövel, Few-Body Syst. **3**, 111 (1988).

[15] S. Galster, H. Klein, J. Moritz, K.H. Schmidt, D. Wegener, and J. Bleckwenn, Nucl. Phys. **B32**, 221 (1971).

[16] M. Gari and W. Krümpelmann, Z. Phys. A **322**, 689 (1985).

[17] S.K. Singh, W. Leidemann, and H. Arenhövel, Z. Phys. A **331**, 509 (1988).

[18] A. Buchmann, W. Leidemann, and H. Arenhövel, Nucl. Phys. **A443**, 726 (1985).

[19] W. Leidemann and H. Arenhövel, Z. Phys. A **326**, 333 (1987); W. Leidemann, K.-M. Schmitt, and H. Arenhövel, Phys. Rev. C **42**, R826 (1990).